Long-term stability and cyclability of a magnesium carbonate hydrate as thermal energy storage (TES) material

Jens Back[a], Ron Zevenhoven[b], Jan-Henrik Smått[c]

[a] Åbo Akademi University, Process and Systems Engineering, Turku, Finland, jens.back@abo.fi
[b] Åbo Akademi University, Process and Systems Engineering, Turku, Finland, ron.zevenhoven@abo.fi, CA
[c] Åbo Akademi University, Molecular Science and Engineering, Turku, Finland, jan-henrik.smatt@abo.fi

Abstract:

As carbon capture and storage (CCS) increasingly transitions toward carbon capture and utilization (CCU), new pathways for the beneficial use of captured CO_2 are required. One promising route is CO_2 mineralisation into magnesium carbonate hydrates (MCHs), which may serve as functional materials beyond permanent storage. Nesquehonite ($MgCO_3 \cdot 3H_2O$) has previously been demonstrated to possess potential as a low-temperature thermochemical thermal energy storage (TES) material operating below 80 °C. This compound can be produced in large quantities via CO_2 mineralisation of abundant magnesium silicate resources, including mine tailings and other industrial waste streams. The reversible dehydration–rehydration reaction, $MgCO_3 \cdot 3H_2O(s) \rightleftharpoons MgCO_3\,(s) + 3\,H_2O(g)$, has a theoretical heat storage density of 1 MJ kg^{-1}.

Building on earlier proof-of-concept work, this study investigates the cyclability, stability, and energy efficiency of nesquehonite-based TES using two experimental approaches. In oven-based experiments, nesquehonite samples were dehydrated at 120 °C for 0.5 h and at 60 °C for 1.5 h, followed by rehydration using liquid water droplets, with material characterization conducted after 20 and 40 cycles. In parallel, two airflow reactor experiments were performed using 10 g and 100 g packed beds. In these experiments, dehydration was achieved by introducing dry hot air to drive an endothermic reaction, followed by cooling and rehydration through humid air exposure, inducing an exothermic heat release.

Temperature profiles and inlet–outlet air humidity measurements were used to assess reaction progression and heat exchange during cycling. The experimental results demonstrate sustained TES performance over repeated cycles, with limited degradation observed under the tested conditions. Thermodynamic equilibrium calculations based on Gibbs free energy minimization, together with scanning electron microscopy (SEM) and X-ray diffraction (XRD) analyses, support the observed phase stability and reversibility. These findings highlight nesquehonite as a promising CCU-derived material for low-temperature thermochemical energy storage applications.

Keywords:

CCS; TES; Magnesium carbonate hydrates; Nesquehonite.

1. Introduction

The concentration of carbon dioxide (CO_2) in the atmosphere has increased steadily since the mid-twentieth century, as evidenced by the longest running direct measurement record from the Mauna Loa Observatory [1]. In February 2026, atmospheric CO_2 levels measured at Mauna Loa, Hawaii, reached 429 parts per million, the highest concentration in at least 2 million years. The most reliable estimates indicate that, from the start of 2020, approximately 500 $GtCO_2$ remained in the carbon budget to have a 50% chance of limiting global warming to 1.5 °C. [2]. Consequently, a broad portfolio of mitigation measures is required, including increased use of low-carbon energy, improvements in energy efficiency, and the deployment of carbon capture and storage or utilisation (CCS/CCU) technologies [3].

In mineral carbonation processes for CO_2 capture and storage through mineralisation (CCSM), large quantities of solid products are generated; typically, one tonne of CO_2 yields 4–5 tonnes of solid material consisting mainly of magnesium carbonate hydrates, amorphous silica, and minor unreacted minerals and metallic oxides

as side streams [3-4]. The development of large-scale applications for these products is therefore essential for improving the overall process economics and enabling a transition from CCS to CCU.

Magnesium carbonate hydrates formed via CO_2 mineralisation are promising functional materials in this context. Nesquehonite ($MgCO_3 \cdot 3H_2O$, below abbreviated to NQ) is of particular interest because it starts to dehydrate at temperatures slightly above 55 °C while retaining sufficient structural integrity to recrystallise upon rehydration [5]. The reversible sorption reaction is given by Eq. 1.

$$MgCO_3(s) + 3H_2O(g) \leftrightarrow MgCO_3 \cdot 3H_2O(s), \qquad \Delta H_{298\,K} = -1.00 \frac{MJ}{kg} MgCO_3 \cdot 3H_2O \tag{1}$$

NQ provides a theoretical, if all crystal water was to sublimate, energy storage density of approximately 1.0 MJ kg^{-1} [6]. This reaction temperature range (50–100 °C) is highly attractive for small-scale and building-application thermal energy storage (TES), where high-temperature thermochemical systems are not suitable or needed [7-8]. In addition, the energy density of magnesium carbonate hydrates is several times higher than that of sensible heat storage in water for typical operating temperature differences. In theory, NQ and Mg carbonate hydrate with five crystal water molecules per $MgCO_3$, called lansfordite ($MgCO_3 \cdot 5H_2O$), can accumulate up to six and eight times more energy, respectively, than heating up a similar mass of water by 40 °C [6]. Although lansfordite has an even higher theoretical storage capacity, it is not viable for practical TES applications because it readily transforms into NQ at room temperature [5-6,9-12].

Compared with other salt hydrates studied for thermochemical heat storage, such as magnesium sulfate ($MgSO_4$), magnesium chloride ($MgCl_2$), and calcium chloride ($CaCl_2$), NQ offers several advantages. It operates at lower temperatures without requiring the sub-atmospheric pressure necessary for some chloride systems, and it inherently incorporates captured CO_2 into the storage material [13-16]. While composite systems (e.g. $MgSO_4$–zeolite) have been developed to improve kinetics and mass transfer [13], these do not provide the additional benefit of CO_2 sequestration that a TES system with NQ does.

More broadly, mineral carbonation using magnesium-bearing materials, widely available as tailings and other waste rock at mining operations, has been identified as a large-capacity and permanent CO_2 storage route, although reaction kinetics, energy demand, and product utilisation remain key challenges [17]. Integrating these materials into TES systems represents a pathway to add value to the mineralisation products while contributing to energy system flexibility.

Thermochemical energy storage based on reversible hydration reactions has been widely recognised as a promising technology for long-term and seasonal heat storage because of its high energy density and negligible heat losses during storage. Recent developments in salt-hydrate systems for building applications have demonstrated the importance of reactor design, heat and mass transfer, and vapour management for achieving stable cyclic performance at low temperatures. In one reported experiment, expanded graphite block impregnated with molten $CaCl_2 \cdot 6H_2O$ was used and cycled as TES material 90 times in a hydration-dehydration reaction. The material remained mechanically and thermally stable without loss of energy density [18]. Compared with other low-temperature salt hydrate systems such as $MgSO_4$ and $CaCl_2$, NQ operates at lower temperatures without deliquescence issues or corrosive chloride chemistry. Furthermore, NQ simultaneously functions as a CO_2 capture and utilisation (CCU) product.

In this work, NQ produced via CO_2 mineralisation was investigated as a thermochemical energy storage material with the dual function of storing heat and utilising captured CO_2. Repeated dehydration–rehydration cycling was carried out using both oven-based and packed-bed airflow configurations to evaluate cyclability, energy efficiency, and structural stability at different scales. By combining temperature and humidity measurements with thermodynamic equilibrium calculations and microstructural characterisation, the study aims to assess the feasibility of NQ-based TES as a large-scale utilisation route for mineral carbonation products.

Two different sets of experiments were conducted. One was a set of oven experiments in a laboratory oven and the second as two series of packed-bed reactor experiment with precise airflow and air humidity control.

2. Experiments in laboratory oven

Two different oven experiments were carried out using a lab-scale oven typically used for drying solid samples. Two temperatures, 120 °C and 60 °C, were used, with two different kinds of NQ products. One of the NQ samples was synthesised from $MgSO_4$(s) and CO_2(g) using ammonia (NH_3(aq)) as pH raising agent, see for example our ECOS2024 paper [20], in the presence of sodium dodecyl sulphate (SDS). The other sample was produced without SDS. The SDS acts as surfactant, and its presence significantly increases the crystal aspect ratio of NQ [20-21].

In the oven experiments, 1 g of NQ was evenly distributed on the surface of a watch glass with a 12 cm radius. The samples were placed into the oven for 30 minutes, followed by cooling for 2 minutes. The crystals were weighed and then rehydrated evenly with 60 water droplets corresponding to 3 ml of H_2O before being placed into the oven again for 30 minutes. Eight such cycles were carried out within a day, and the samples were left in rehydrated state overnight (after 8, 16, 24, 32 and 40 cycles). One batch of samples were cycled 20 times and another 40 times.

2.1. Weight analysis of the TES material during oven cycles

The mass difference between the cycles for the 120°C series is presented in Figure 1 (left) where the final measurement value, cycle number 41 is the mass value for the rehydrated (and dried overnight) sample.

Half of the samples were left in the dehydrated stage and half were rehydrated with the same amount of water as during cycling. The final mass difference between the rehydrated and dehydrated samples is given in Table 1. The NQ sample produced with some SDS shows a more continuous mass loss than the NQ produced without SDS, most likely as a result of a less uniform structure for the latter. The cycling experiment at 120 °C led to a mass loss of 24.98 % to 31.61 % in the samples; apparently the material is converted to a mixture of hydromagnesite $4MgCO_3 \cdot Mg(OH)_2 \cdot 4H_2O$, dypingite $4MgCO_3 \cdot Mg(OH)_2 \cdot 5H_2O$ and magnesite $MgCO_3$.

The experiment series was repeated with the oven at 60 °C. To completely dry the samples, i.e. to get rid of any excess moisture, the samples had to stay 90 minutes in the oven. Five cycles were made in a day, and the samples were left in rehydrated state overnight. The mass difference between the cycles is presented in Figure 1 (right) where the final value, cycle number 41 is the mass value for the rehydrated (and dried overnight) sample.

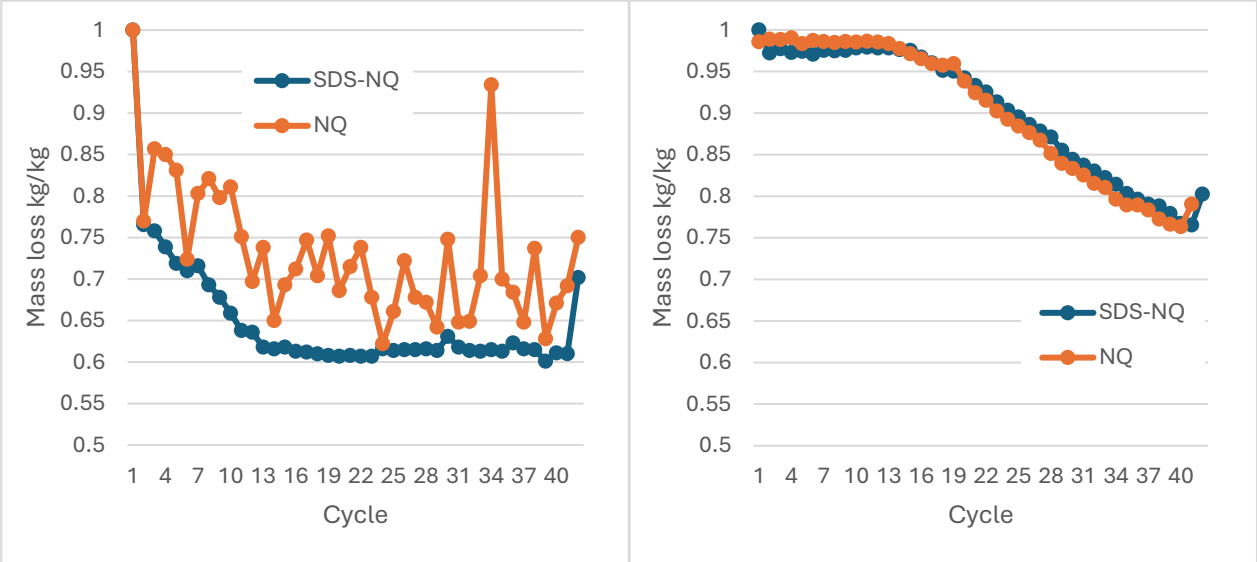

Figure 1. *Mass loss over the 40 cycles at 120 °C (left) and 60 °C (right).*

Table 1. *Final masses for the samples in the 120 °C and the 60 °C oven experiment respectively.*

	120 °C oven experiment			60 °C oven experiment		
Experiment	Weight directly after last oven cycle (g)	Weight rehyd & dried or after cooling (g)	Mass difference after cooling/ rehydration overnight (%)	Weight directly after last oven cycle (g)	Weight rehyd & dried or after cooling (g)	Mass difference after cooling/ rehydration overnight (%)
SDS NQ rehyd 40	0.6101	0.7019	-29.81	0.7653	0.8025	-19.75
SDS NQ dehyd 40	0.6419	0.6839	-31.61	0.7715	0.7969	-20.31
SDS NQ rehyd 20	0.6399	0.7354	-26.46	0.9392	0.9523	-4.77
SDS NQ dehyd 20	0.6550	0.6950	-30.50	0.9529	0.9634	-3.66
NQ rehyd 40	0.6919	0.7502	-24.98	0.7634	0.7904	-20.96
NQ dehyd 40	0.6744	0.7089	-29.11	0.8062	0.8212	-17.88
NQ rehyd 20	0.6486	0.7459	-25.41	0.9166	0.9224	-7.76
NQ dehyd 20	0.6555	0.7006	-29.94	0.9150	0.9249	-7.51

Half of the samples were left in the dehydrated stage and half were rehydrated with the same amount of water as during cycling. The final mass difference in the rehydrated and dehydrated samples for the 60 °C experiment is given in Table 1 as well. The cycling experiment at 60 °C led to a mass loss of 3.66 % to eventually 20.96 %.

2.2. SEM image analysis of the TES material during/after oven cycles

Eight different samples for each tested oven temperature experiments were taken to visual analysis using SEM; rehydrated as well as rehydrated samples after 20 and 40 cycles, respectively.

Figure 2 gives the NQ sample for the 120°C test, showing that the fibrous structure of the NQ has been transformed significantly. The flake-like structures, seen in the SEM pictures in sphere formations, are characteristic of magnesium carbonate ($MgCO_3$), suggesting that much of the NQ has been transformed into $MgCO_3$. This observation is consistent with earlier thermogravimetric studies showing that elevated temperatures promote irreversible structural rearrangement and densification of Mg-carbonates [5]. The same was seen (no figure given here as the image looks very much the same) with the SDS-NQ sample.

The original NQ samples before the tests are shown in Figure 3, showing the fibrous structure that is more difficult to recognise in Figure 2.

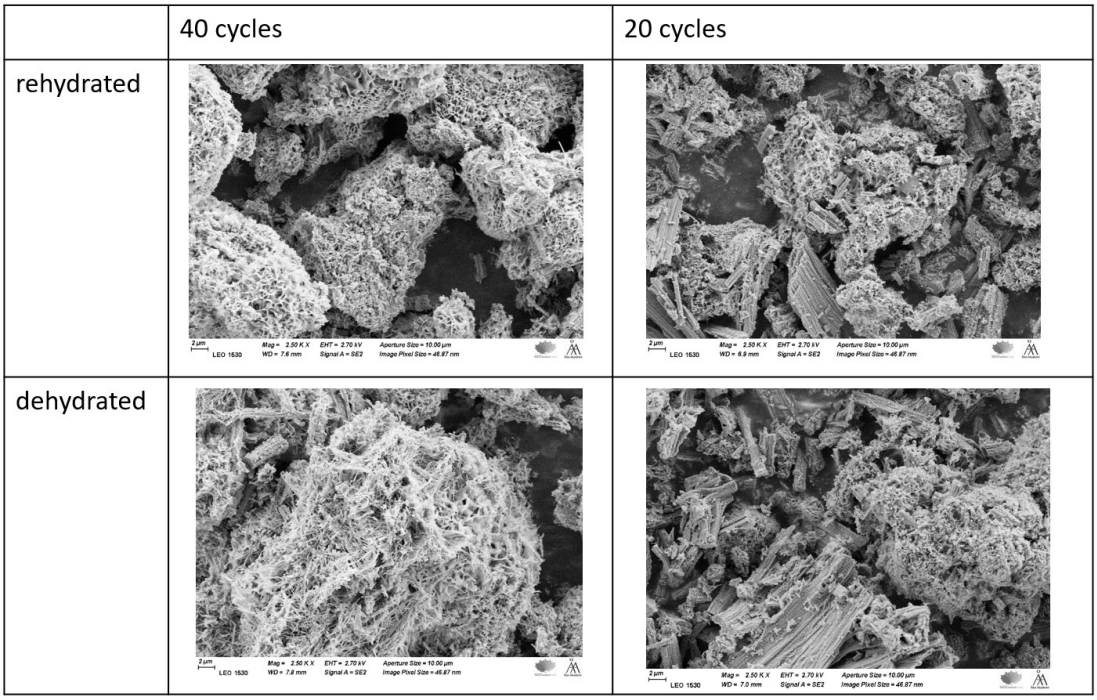

Figure 2. *SEM pictures of NQ after 40 cycles and 20 cycles in 120 °C oven experiment in 2 500 times magnification.*

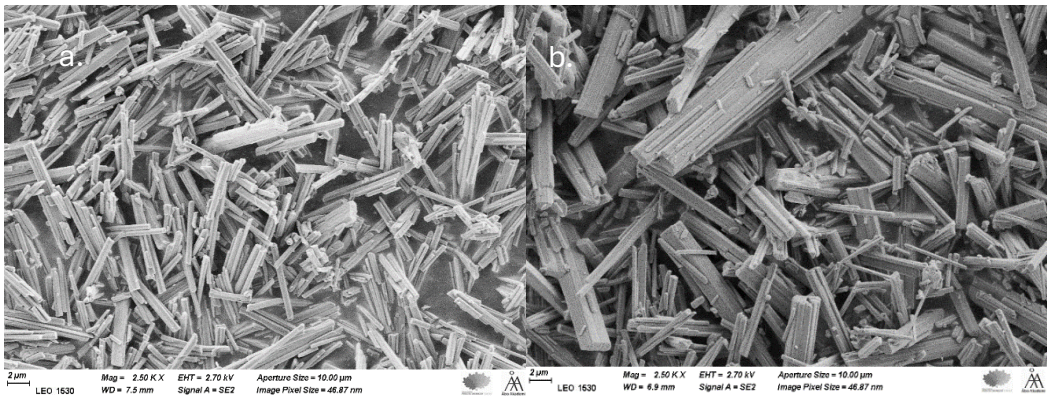

Figure 3. *SEM pictures of original NQ product before oven experiments. a. SDS-NQ b. NQ. 2 500 times magnification.*

Figures 4 and 5 give the images obtained for the 60 °C oven experiments. In these figures, the rod-like structures of NQ are much more prominent, albeit the NQ has decomposed to $MgCO_3$ to some degree. No clear difference can be seen between the rehydrated and dehydrated samples. The results indicate that although complete dehydration can theoretically enhance energy density, operation at moderate temperatures

is preferable for long-term cyclic stability. For practical TES applications, excessive dehydration severity may therefore compromise cyclability by promoting irreversible phase transitions.

	40 cycles	20 cycles
rehydrated	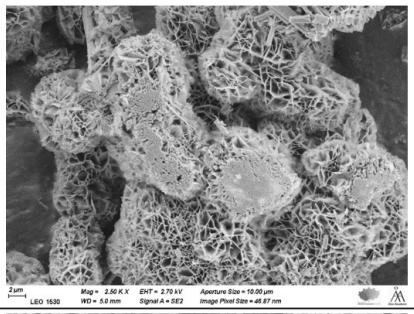	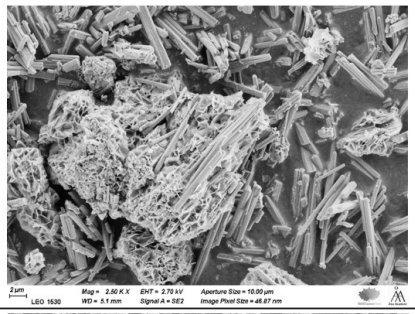
dehydrated	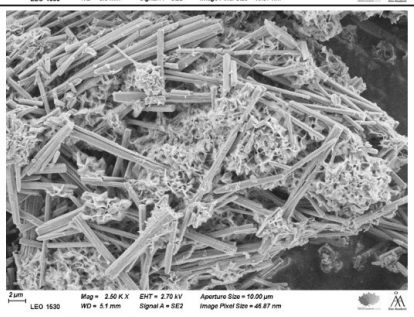	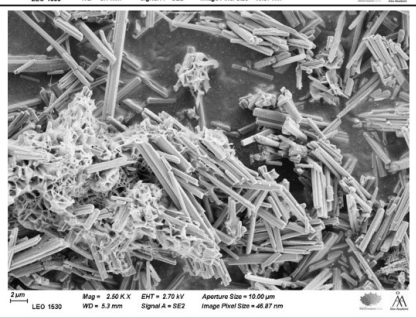

Figure 4. *SEM pictures of SDS-NQ after 40 cycles and 20 cycles in 60 °C oven experiment in 2 500 times magnification.*

	40 cycles	20 cycles
rehydrated	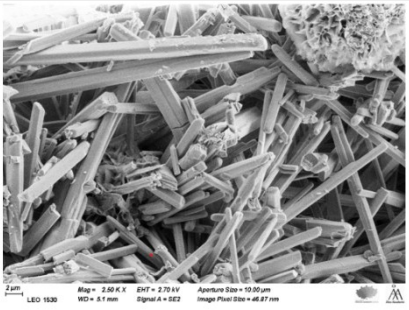	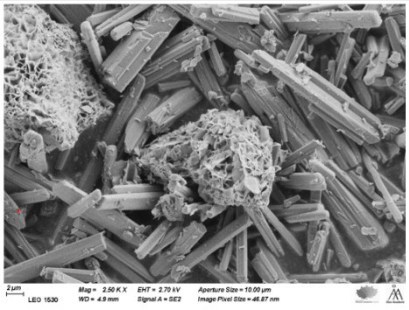
dehydrated	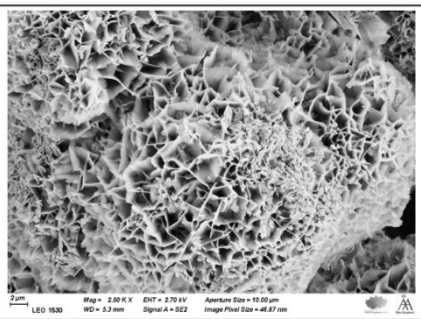	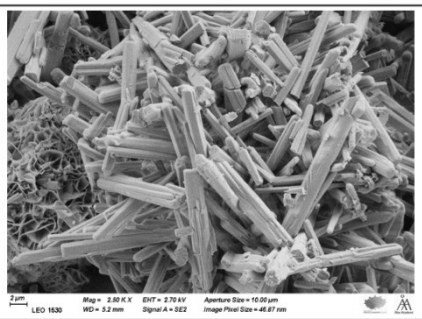

Figure 5. *SEM pictures of NQ after 40 cycles and 20 cycles in 60 °C oven experiment in 2 500 times magnification.*

3. Experiments with controlled airflow and inlet humidity

3.1. Experimental set-up and procedure

Based on the results from the oven experiments, a second experiment series was designed. Instead of water droplets, a controlled flow of humid air was used to better simulate the real conditions of a commercial TES-system. The second aim was to use temperature and air flow humidity measurements to quantify performance based on mass and energy balances.

A packed bed column reactor was designed inside an aluminium cylinder with the gas inlet at the bottom and outlet at the top. The inlets and outlets were drilled through plastic lids. The bed of NQ was kept in place by two plastic discs with holes in them for sufficient airflow through the bed. Beneath the bed an air chamber reassured even spread of the airflow from the inlet. Above the bed there was a second air chamber to fit the humidity probe. Furthermore, three thermocouples were used to monitor temperatures: one in the bottom chamber, one in the middle of the bed, and one in the top chamber. All this was kept inside a 4 cm-thick Styrofoam mantle, tightly encapsulating the column. The air flow and humidity were controlled with a Cellkraft P-Series humidifier coupled to the inlet of the reactor. A schematic picture of the packed-bed reactor is given in Figure 6.

Two sets of experiments were conducted with this setup. The parameters for the experiments are given in Table 2, with code X for the experiment with 10 g NQ for 40 cycles and code C for with 100 g NQ for 10 cycles.

Cooling of the system after a dehydration step before a rehydration step happened overnight.

***Figure 6**. Schematic picture of the packed-bed reactor with humidity probe and thermocouples.*

***Table 2.** Parameters for the airflow experiments.*

Experiment ID	X	C
NQ used	10 g	100 g
NQ bed height	8 mm	8 cm
Dehydration cycle duration and airflow	3 h and 3.5 L/min	6 h and 3 L/min
Rehydration cycle duration and airflow	1.5 h and 2 L/min	24 h and 2 L/min
Completed cycles	40	10 (+½)

In the X experiment, 0.5 g of NQ was taken out after 10 cycles for analysis. The NQ used in experiment X was synthesized in the presence of SDS whilst the NQ in experiment C was not. Due to the larger sample mass in experiment C, the dehydration airflow rate was lowered to 3 L/min since a slight pressure disturbance was noticed with the 3.5 L/min flow. The aim was to obtain a bed temperature 60 °C during the dehydration step. In the X experiment, this was reached after approximately 35 min and in the C experiment after 4-5 h. For the rehydration, humid air was used produced by the Cellkraft humid air generator. A 2 vol-% humidity was used corresponding to an approximate relative humidity of 77% in all rehydration cycles. After the 10^{th} cycle of the C experiment, 50 g of the NQ was further put through a 11^{th} heat up cycle and a sample of this dehydrated NQ was also analysed.

The temperature curve of the bed of every 4^{th} rehydration cycle of the X experiment can be seen in Figure 8. The heat curve of the bed of every rehydration cycle of the C experiment can be seen in Figure 9. The longer cooling time of cycle number 10 can be explained by the ambient temperature being clearly higher in the laboratory for this particular run with a starting temperature of 20.8 °C compared to a mean of 19.8 °C for the rest of the trials.

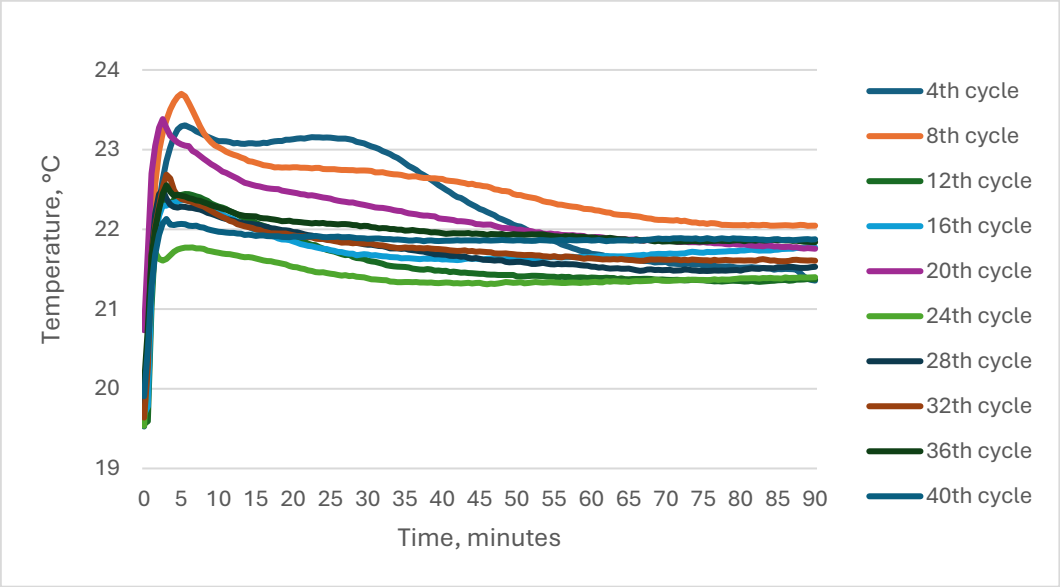

Figure 8. *Temperature of the bed in every 4th rehydration cycle in experiment X as a function of time.*

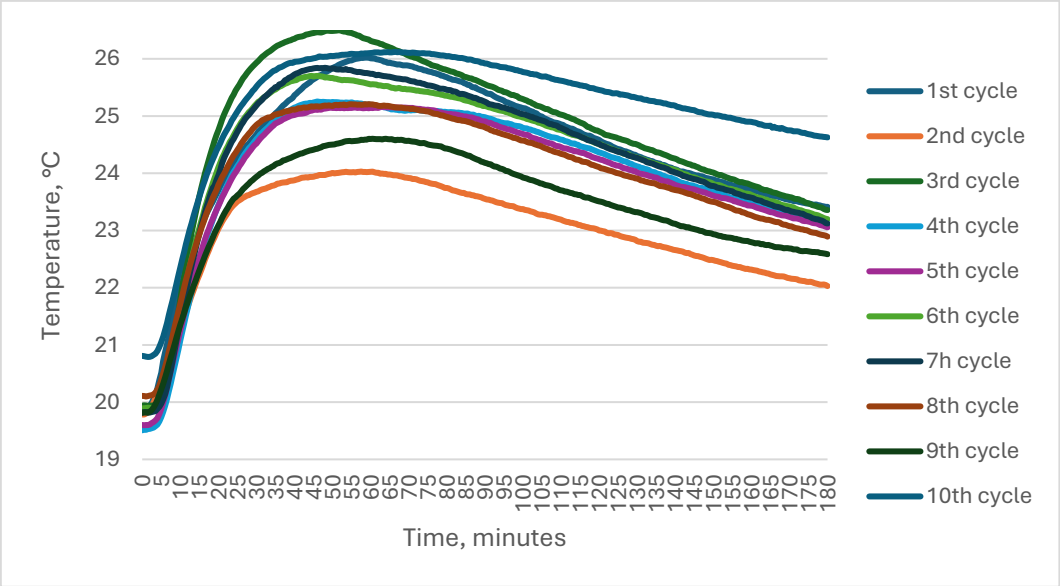

Figure 9. *Temperature of the bed in every rehydration cycle in experiment C as a function of time.*

3.2. Results: analysis of NQ from the steam generator experiments

The different samples from the experiments were taken to SEM and XRD analysis, as shown below in Figures 10 and 11, respectively.

In Figure 10, the observable crystals in all four different pictures are characteristic to NQ. However, the XRD diffractogram for the X experiment, see Figure 11 (left) shows some $MgSO_4 \cdot 6H_2O$ (the precursor for the earlier produced NQ) as the only crystalline species present. The broad reflections at ~16.9, 27.4, 32.2, and 49.0° could correspond to a poorly crystalline basic magnesium hydroxy carbonate–sulfate hydrate. Earlier work by Sun et al. showed a similar diffractogram claiming to show NQ [22]. The diffractogram for the C experiment, see Figure 11 (right) shows NQ present along with some epsomite ($MgSO_4 \cdot 7H_2O$), which is also a precursor used for producing NQ.

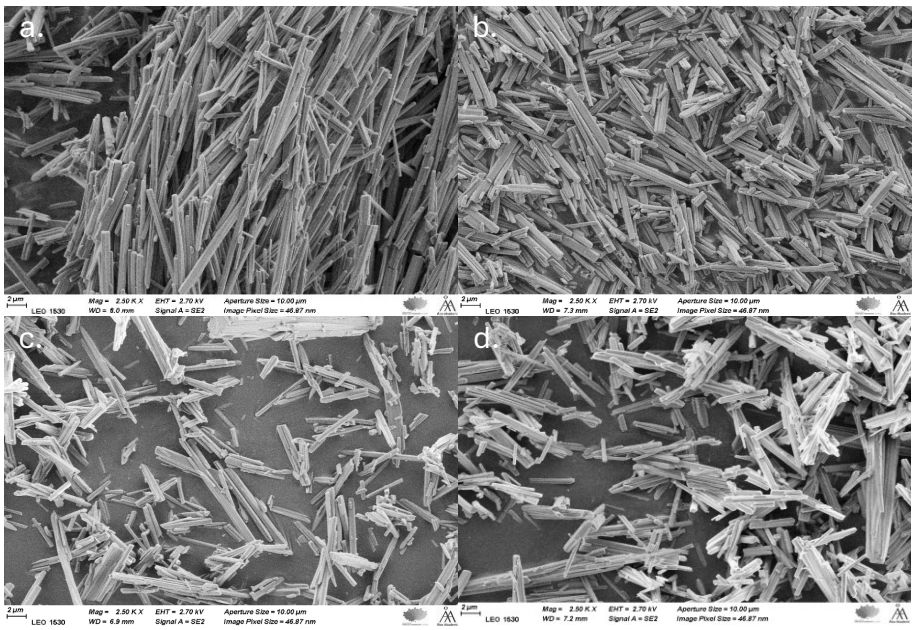

Figure 10. *SEM pictures of the NQ from the steam generator tests in 2 500 times magnification. a. SDS-NQ after 10 cycles in the X experiment, b. SDS-NQ after 40 cycles in the X experiment, c. NQ after 10 cycles in the C experiment, d. NQ after the 11th heat up cycle in the C experiment*

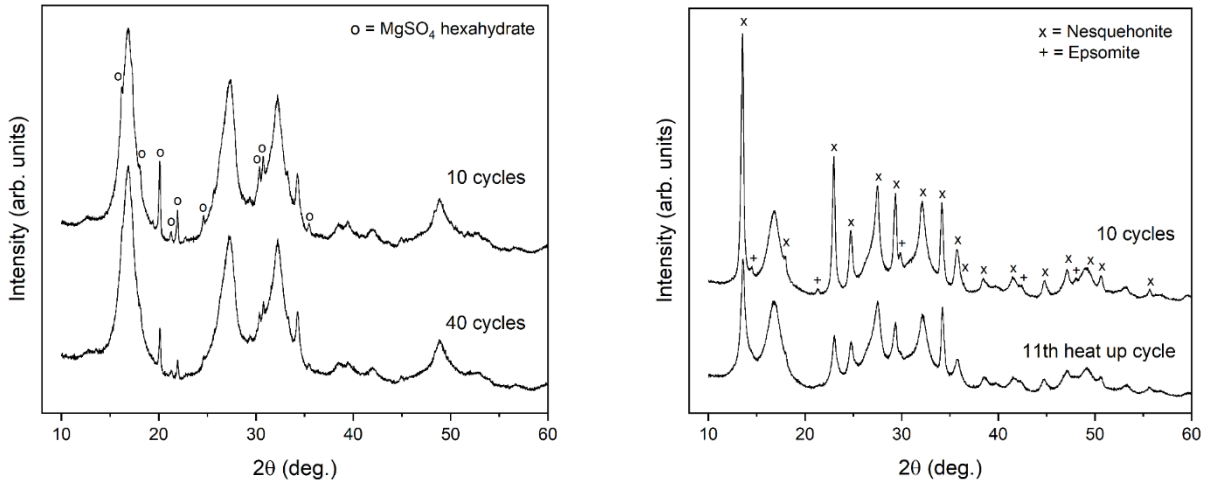

Figure 11. *XRD pattern for the NQ from experiment series X (left). The upper curve shows the pattern for the sample after 10 cycles and the lower curve after the full 40 cycles. XRD pattern for the NQ from experiment series C (right). The upper curve shows the pattern for the sample after 10 cycles and the lower curve after the 11th heat up cycle*

3.3. Results: heat storage performance during cycling

By integrating over time and knowing the input and output airflow, as well as the temperature and humidity of these, the energetic effects of the water loss from the TES material can be calculated. The same approach can be used to determine the energetic effects of water uptake by the TES material during the rehydration cycle. Dry air and water vapour are assumed to be ideal gases with specific heat capacity c_p = 1.006 kJ/kg·K and 1.84 kJ/kg·K, respectively. Having no liquid water in the system anywhere, the enthalpy h of dry air and water vapour are taken at h = 0 at T = 0 °C. This was used to calculate the energy released or taken up during hydration/ dehydration cycles according to Eq. (2).

For the container system shown in Figure 6, composed of PVC and aluminium both having a specific heat capacity of 900 J/kg·K and a combined mass of 373.5 g, the energy for heat up can be calculated separately. Likewise for the heat up of the NQ material, apart from the TES effect being analysed, the heat for raising the temperature was calculated using, for the temperature range 20–70 °C, a specific heat capacity of 57 cal/mol·K [23] which corresponds to 1723.7 kJ/kg·K – see Eqs. (3) and (4).

The heat effect of the actual dehydration or hydration (rehydration) reaction, see Eq. (1) was calculated using HSC chemistry [6] to be around 168 kJ/mol for the temperature range considered, which corresponds to 1.214

MJ/kg NQ for complete loss and regain of $3H_2O$ crystal water. Using Eq. (5) the degrees of conversion were calculated based on the energy effect while Eq. (6) was used to calculate the amount of moisture given off or taken up by the TES material. This could be compared with a maximum effect of 390.85 g H_2O per kg NQ, giving a degree of conversion base on mass, evaluated at Δt = 30 s intervals during 3 h for dehydration or 6 h for hydration, respectively.

$$energy\ stored\ in\ TES\ system = \dot{m}_{dry\ air} \cdot \{(1.006 \cdot (T_{in} - T_{out}) + (1.84 \cdot (\omega_{in} \cdot T_{in} - \omega_{out} \cdot T_{out}))\} \quad (2)$$

$$\begin{aligned} energy\ effect\ of\ TES\ hydration\ or\ dehydration & \\ = energy\ stored\ in\ TES\ system & \\ - energy\ for\ heating\ or\ cooling\ container\ and\ TES\ material & \end{aligned} \quad (3)$$

$$energy\ for\ heating\ or\ cooling\ the\ container\ and\ the\ TES\ material = m \cdot c_p \cdot (T_{end} - T_{start}) \quad (4)$$

$$degree\ of\ conversion\ based\ on\ energy = \frac{energy\ effect\ of\ TES\ hydration\ or\ dehydration}{1.214\ \frac{MJ}{kg\ NQ}} \quad (5)$$

$$\Delta m_{H2O} = \sum_i \dot{m}_{dry\ air} \cdot (\omega_{end,i} - \omega_{start,i}) \cdot \Delta t \quad (6)$$

$$degree\ of\ conversion\ based\ on\ mass = \frac{\Delta m_{H2O}}{3.91\ g\ (10\ g)\ or\ 39.10\ g\ (100g)} \quad (7)$$

A typical curve for measured water vapour release and enthalpies of air entering and leaving the TES material during a dehydration is given in Figure 12. The highest point of the “enthalpy in flow” curve corresponds to dry air at 74.5 °C. The first 15 minutes of moisture release were interpolated using a logarithmic mean function because of a non-linear fast start of the process. For the experiment shown in Figure 12, the dehydration was still ongoing after three hours while the thermal effects appeared to have stabilized at constant (temperature) levels with moisture contributing less to the outgoing air flow enthalpy.

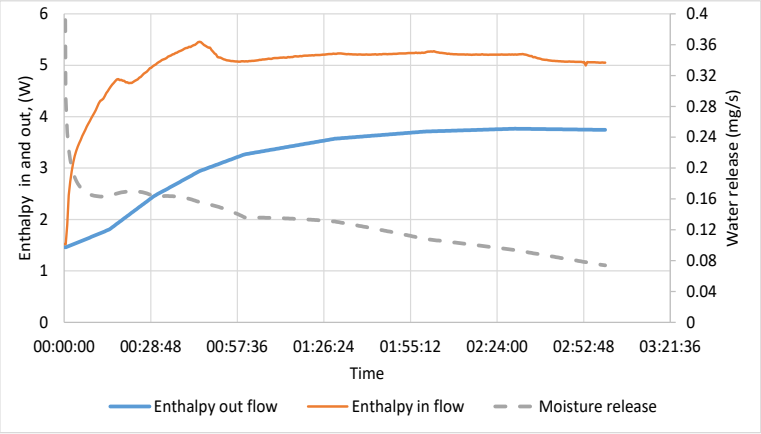

Figure 12. *Dehydration, moisture release and enthalpy for the 2nd cycle, series X.*

The cycling results as degrees of TES material conversion during the 10 cycles C and 40 cycles X series are given in Figures 13a and b, respectively, giving mass and energy effects quantified as degrees of conversion for moisture release according to Eqs. (5) and (7).

Results obtained with larger NQ amounts (series C) show a more stable trend although a difference exists between moisture mass loss and the energy effect that mass loss would give in theory based on the thermochemical TES effect that is studied. For this series, a consistent release of around 10% of the theoretical moisture release was found. The thermal effect show a decline after the 7th cycle.

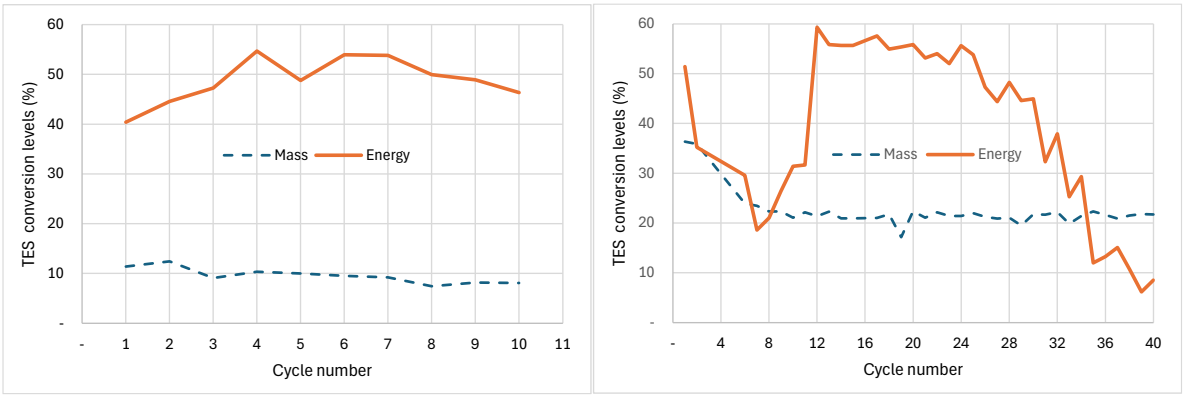

Figure 13. *Degrees of conversion during dehydration based on series C (left) and series X (right).*

For the X series with only 10 g NQ starting material, moisture releases drop from around 35% of the theoretical value to a value stabilizing at around 20% of the theoretical value. A rather dramatic fluctuation is seen in the energy effect: after an initial drop, a sudden rise to 60% of the theoretical energetic TES effect for complete release of $3H_2O$ from the NQ crystal structure. (Note that after the 10th cycle the system was opened and closed for taking out a small amount of TES material for analysis.) After the 17th cycle, the energetic effect starts to drop and further drcreases to below 10% of theoretical values after the 40th cycle.

Both test series suggest that water transformed from crystal water to absorbed moisture, which does give a heat effect but no release of water with the outgoing air flow.

Table 3. *Degrees of conversion during dehydration based on series C (left) and series X (right).*

Experiment series	X	C
Moisture release	0.84 +/- 0.15 g	3.75 +/- 0.57 g
(average +/- standard deviation)	22.3 +/- 3.3 %	9.57 +/- 1.47 %
TES energy effect	4.67 +/- 2.03 kJ	59.33 +/- 5.22 kJ
(average +/- standard deviation)	487.7 +/- 215 kJ/kg NQ	593.3 +/- 52.2 kJ/kg NQ

Table 3 summarizes the results of the dehydration tests. The larger bed required 4–5 h to reach 60 °C, compared to ~35 min for the smaller bed. This reflects: 1) Increased internal heat transfer resistance and 2) slower vapour diffusion through the packed structure. This suggests that reactor engineering - particularly airflow distribution, bed porosity, and thermal conductivity enhancement - are critical for scale-up. In this respect, incorporation of conductive matrices (e.g. expanded graphite), as reported for $CaCl_2$ systems [24], could improve heat transfer without compromising chemical stability.

For the hydration tests, humid air at 20 °C at 2 vol-% H_2O at a flow rate of 2 L/min (87 % relative humidity, ω = 12.4 g H_2O / kg dry air specific humidity) was produced by the Cellkraft humidifier, corresponding to a moisture feed of around 36 mg/min. A result figure on enthalpy in- and outflows and moisture from the TES system is given in Figure 14.

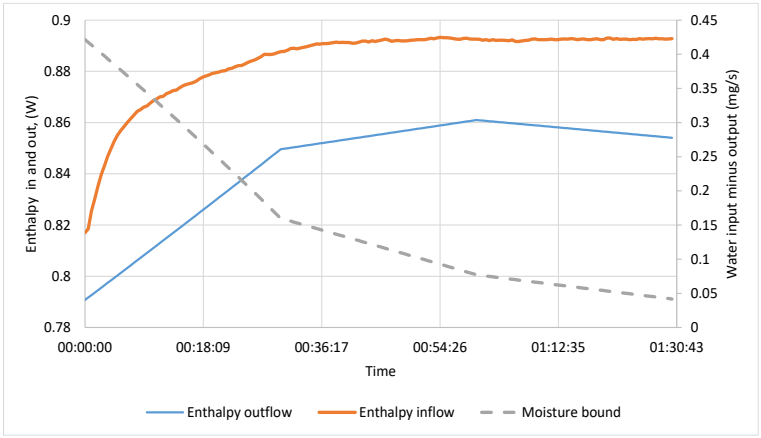

Figure 14. *Hydration, moisture release and enthalpy for the 2nd cycle, series X.*

Calculating the energy release to the outgoing air flow gives a value of 0.22 kJ with total uptake of water for the rehydration equal to 0.72 g based on the varying conditions immediately before and after the NQ bed. This is around half of the water observed to be released in the heat up step. (Using the constant temperature and humidity air flow from the Cellkraft for the calculation gives a total uptake of water equal to 0.86 g.).

The energy released did, however, not result in the enthalpy of the air flow leaving being higher than that of the air flow entering: temperature changes of the TES material from 19.7 °C to 23.5 °C followed by a decrease to 21.5 °C overruled this effect. As a result, the 0.22 kJ heat released is < 3% of the TES heat release potential which at around 20°C is 118.8 kJ/mol NQ, or 8.59 kJ for 10 g material

4. Conclusions

The present study evaluated NQ as a thermochemical TES material produced via CO_2 mineralisation, with emphasis on long-term cyclability, phase stability and heat storage performance under low-temperature operating conditions.

Oven experiments clearly demonstrated that dehydration temperature strongly influences long-term material stability. At 120 °C, a significant mass loss (25–32%) was observed after 40 cycles; apparently the material is converted to a mixture of hydromagnesite $4MgCO_3{\cdot}Mg(OH)_2{\cdot}4H_2O$, dypingite $4MgCO_3{\cdot}Mg(OH)_2{\cdot}5H_2O$ and magnesite $MgCO_3$. SEM analysis indicates partial transformation of NQ into magnesite. At 60 °C, mass losses were substantially lower (4–21%), and rod-like NQ structures remained dominant in SEM images. This confirms that dehydration near the lower thermodynamic boundary of the NQ ⇌ magnesite equilibrium better preserves structural reversibility.

In the controlled air flow and packed-bed system, SEM images show predominantly NQ crystals even after 40 cycles (experiment X) and 10+1 cycles (experiment C). No clear magnesite morphology was detected. suggesting that vapour-phase hydration provides more homogeneous mass transfer compared with droplet-based rehydration. This highlights a key design consideration for practical systems: liquid-phase rehydration may induce partial recrystallisation pathways leading to phase segregation, whereas vapour-based hydration supports a more reversible processing.

Humidity integration and enthalpy calculations indicate an average water release of ranging from 60% to below 10% of the theoretical maximum energy (TES material) effect for dehydration with 10 g NQ material, against values ranging from 40% to 55% for the dehydration of 100 g NQ material. When calculated based on water release, the conversion is smaller at around 20% and 10% of theoretical values. Apparently, water transformed from crystal water to absorbed moisture, giving a heat effect but no release of water with the outgoing air flow.

The findings suggest that: 1) The effective enthalpy change may include additional structural or adsorption-related contributions, and/or 2) experimental uncertainties overestimate water release. Nevertheless, reasonably stable cyclic performance was seen for the tests with 100 g NQ.

From a carbon capture and utilisation (CCU) perspective, the study demonstrates that nesquehonite produced via mineral carbonation can function as a reversible TES medium under mild conditions (≈50–80 °C). This temperature window is highly compatible with solar thermal collectors, industrial waste heat recovery, district heating return flows, and building-level seasonal heat storage. The dual functionality - CO_2 mineral storage combined with thermal storage - improves the economic case for large-scale mineral carbonation. Since mineralisation produces several tonnes of solid product per tonne CO_2 captured, identifying high-volume applications is essential. TES represents one such opportunity. However, long-term durability beyond 40 cycles and operation under fluctuating humidity conditions require further study. Additionally, the XRD indication of residual $MgSO_4$ and epsomite suggests that precursor purity and synthesis pathway influence TES performance and should be optimised.

Nomenclature

$CaCl_2$	Calcium chloride	SDS	Sodium Dodecyl Sulfate
CCS	Carbon Capture and Storage	SEM	Scanning Electron Microscopy
CCSM	CCS through Mineralisation	TES	Thermal Energy Storage
CCU	Carbon Capture and Utilisation	XRD	X-ray Diffraction
CO_2	Carbon Dioxide	c_p	Specific heat capacity J/(kg·K)
MCH	Magnesium Carbonate Hydrate	h	Specific enthalpy J/kg
$MgCl_2$	Magnesium Chloride	L	Litre
$MgCO_3$	Magnesite	min	Minutes
$MgCO_3{\cdot}5H_2O$	Lansfordite	m, $\dot{m}$	Mass flow kg, kg/s
$MgSO_4$	Magnesium Sulfate	t	Time s
NH_3	Ammonia	T	Temperature °C
NQ	Nesquehonite ($MgCO_3{\cdot}3H_2O$)	ω	Specific humidity kg H_2O / kg dry air

References

[1] Lan, X., Tans, P., Thoning, K.W.: Trends in globally-averaged CO_2 determined from NOAA Global Monitoring Laboratory measurements. Version Thursday. 05-Feb-2026 14:41:21 MST https://doi.org/10.15138/9N0H-ZH07 (accessed 12.2.2026)

[2] IPCC. 2023: Climate Change 2023: Synthesis Report. Contribution of Working Groups I. II and III to the Sixth Assessment Report of the Intergovernmental Panel on Climate Change

[3] Metz, B., Davidson, O., de Coninck, H., Loos, M., Meyer, L., 2005, IPCC special report on carbon dioxide capture and storage. *Cambridge University Press*. United Kingdom and New York. NY. USA.

[4] Zevenhoven, R., Back, J., Fagerlund, J., Sorjonen-Ward, P., Mineral Carbonation using Mine Tailings – A Strategic Overview of Potential and Opportunities, preface by Craig, J.: IEAGHG Technical Report: 2022-10, Cheltenham, UK: International Energy Agency, 123 s.

[5] Jauffret, G., Morrison, J., Glasser. F.P., 2015, On the thermal decomposition of nesquehonite. *J. Therm. Anal. Calorim*. 122. 2: 601–609.

[6] Outotec. 2014. HSC Chemistry 8.1.1 – Reaction equations database. *Outotec Research Oy*.

[7] Erlund, R., Zevenhoven, R., 2018, Hydration of magnesium carbonate in a thermal energy storage process and its heating application design. *Energies*. 11. 1: 170–185.

[8] N'Tsoukpoe, K.E., Liu, H., Le Pierrès, N., Luo. L., 2009, A review on long-term sorption solar energy storage. *Renew. Sustain. Energy Rev.* 13. 9: 2385–2396.

[9] Hill. R.J., Canterford, J.H., Moyle. F.J., 1982, New data for lansfordite. *Mineral. Mag.* 46. 341: 453–457.

[10] Hopkinson, L., Kristova, P., Rutt, K., Cressey, G., 2012, Phase transitions in the system MgO–CO_2–H_2O during CO_2 degassing of Mg-bearing solutions. *Geochim. Cosmochim. Acta*. 76: 1–13.

[11] Dell, R.M., Weller, S.W., 1959, The thermal decomposition of nesquehonite $MgCO_3 \cdot 3H_2O$ and magnesium ammonium carbonate. *Trans. Faraday Soc.,* 55: 2203–2220.

[12] Ming. D.W., Franklin. W.T., 1985. Synthesis and characterization of lansfordite and nesquehonite. *Soil Sci. Soc. Am. J.,* 49. 5: 1303–1308.

[13] Hongois, S., Kuznik, F., Stevens, P., Roux, J.J., 2011, Development and characterization of a new $MgSO_4$–zeolite composite for long-term thermal energy storage. *Sol. Energy Mater. Sol. Cells*. 95. 7: 1831–1837.

[14] Morgan, B., Wilson, S., Madsen, I., Gozukara, J., 2015, Increased thermal stability of nesquehonite in the presence of humidity and CO_2: Implications for low-temperature CO_2 storage. *Int. J. Greenh. Gas Control*. 39: 366–376.

[15] Erlund, R., Zevenhoven, R., 2017, Thermal storage of (solar) energy by sorption of water in magnesium (hydro)carbonates. *Int. J. Thermodyn.,* 20. 2: 102–109.

[16] Lele, A.F., Kuznik, F., Rammelberg, H.U., Schmidt, T., Ruck, W.K.L., 2015, Thermal decomposition kinetic of salt hydrates for heat storage systems. *Appl. Energy*. 154: 447–458.

[17] Bobicki, E. R., Liu, Q., Xu, Z., Zeng, H., 2012, Carbon capture and storage using alkaline industrial wastes. *Can. J. Chem. Eng*., 90. 3: 547–572

[18] Galazutdinova, Y., Clark, R.-J., Al-Hallaj, S., Kaur, S., Farid, M., 2024, New Thermochemical Salt Hydrate System for Energy Storage in Buildings. *Energies*. *17*(20). 5228

[19] Back, J., Ismailov, A., Sreenivasan, H., Smått, J.-H., Santos, H.S., Nguyen, H., Levänen, E., Zevenhoven, R., Kinnunen, P., 2025, Influence of additives. temperature. and pressure on the morphology of nesquehonite– results from three synthesis routes. *Emergent Mater.,* 8. 2853 —2868

[20] Back, J., Koivisto, E., Zevenhoven, R., Consequences of alkaline salt choice for pH raise during CO_2 mineralisation using rock-derived magnesium salt. Proc. of ECOS2024 37th Int. conf. on efficiency, cost, optimization, simulation and environmental impact of energy systems June 30 – July 5, 2024, Rhodes, Greece. Karellas, S., Roumpedakis, T. & Braimakis, K. (Eds.) Paper 340.

[21] Geng. X., Lv, L., Zhang, T., Tang, S., 2020, The regulating mechanism of $MgCO_3 \cdot 3H_2O$ whisker growth orientation with the presence of SDS. *J. of CO_2 Utiliz.*, 42

[22] Sun, B., Zhou, H., Arovo, M., Chen, J., Chen, J., Shao, L., 2015, Preparation of basic magnesium carbonate by simultaneous absorption of NH_3 and CO_2 into $MgCl_2$ solution in an RPB. *Powder Technol.*, 284: 57-62.

[23] Robie, R.A., Hemingway, B.S. 1972 The Heat capacities at low-temperatures and entropies at 298.15 K of nesquehonite, $MgCO_3$-$3H_2O$, and hydromagnesite. *Amer. Mineralogist*, 57, 11–12: 1768–1781

[24] Reynolds, J., Abbas, B., Sullivan, G., Elvins, J., Jewell, E., Searle J., Skevi, L., Ke, X. 2024. Optimisation of $CaCl_2$ impregnated expanded graphite and alginate matrices – Targeted salt loading. *Energy Conv, Manage*. 302: 118145

Acknowledgements

The authors acknowledge the Research Council of Finland (MAGNEX 2022-2025, project 347183) and K.H. Renlund's foundation (2025) for the funding of this work. We acknowledge our colleagues Linus Silvander and dr. Emil Vainio for SEM analysis and support with the humid / heated air flow generator.